A modified PQ method for dual stage instrumented suspension control design

A Modified PQ Method for Dual Stage Instrumented Suspension Control Design

Rudy Oosterbosch

DCT 2004.88

Traineeship report

Coach: R. A. de Callafon (UCSD)

Supervisor: M. Steinbuch (TU/e)

University of California San Diego (UCSD), La Jolla, USA
Department of Mechanical and Aerospace Engineering
System Identification and Control Group

Technische Universiteit Eindhoven (TU/e)
Department of Mechanical Engineering
Dynamics and Control Technology Group

Eindhoven, August, 2004

Abstract

For attenuating a high frequent windage disturbance in a hard disk drive system, a dual stage instrumented suspension is used with a low bandwidth large-stroke actuator and a high bandwidth short-stroke actuator. A high bandwidth controller for attenuating the high frequent windage disturbance already exist. The remaining problem is that destructive motion may occur when seeking or following a track because the two actuators act in parallel. To offer a solution for this problem when using two different bandwidth actuators, a dual stage controller can be designed by using the PQ method. Since there are restrictions to the working range of each actuator a modification to the PQ method is made by explicitly considering these restrictions. This report presents that the modified PQ method will give good and acceptable results for the dual stage controller design.

Contents

Chapter 1

Introduction

A hard disk drive uses stacks of co-rotating magnetic disks to store data in concentric circular tracks. The data is read and written to the disk by means of a read/write head mounted at a tip of a suspension. The suspension is moved across the surface of the disk by an actuator. A head-positioning servo system maintains the head position along the center of the tracks on the disk and provides the movement of the head from one track to another by driven the actuator.

A trend in magnetic disk drives is that the storage capacity is increasing rapidly while access time to data stored on the disk is being reduced. To reduce access time, a larger rotational disk spindle speed has been imposed. The high rotational speed causes a large windage disturbance and disk flutter, which are serious obstacles in increasing the track density of hard disk drives. Since the disturbances cause high frequent vibrations an effective method to achieve a higher track density is to increase the control system bandwidth. The higher the bandwidth the larger the disturbance reduction below the bandwidth.

Because of limitations of a single stage suspension here a dual stage suspension is used. Using a dual stage suspension lowers the inertia and the power requirements [1]. Because of the bandwidth limitations of a Voice Coil Motor (VCM) actuation here two actuators act in parallel. A VCM is still used as an actuator for the first stage to generate a large but coarse and slow movement, while a piezoelectric Micro Actuator (MA) is used as an actuator for the secondary stage to provide fine a fast positioning. Now high suspension resonances can be attenuated by using the MA. In [2] and [3] a fast actuation servo controller has been suggested for compensating windage induced disturbances of the imposed increase in rotational disk spindle speed.

Reducing track mis-registration in a hard disk drive system by high bandwidth digital control implies fast sampling of the track mis-registration but, in most drives, the sampling frequency of the track mis-registration is limited to 15-20 kHz. To provide the control system with high frequent information for high bandwidth control an additional sensor is instrumented on the suspension for an indirect measurement of the track mis-registration. This sensor is of a piezo-resistive material and can be used for measuring high frequent vibrations at a sample frequency of 50 kHz. In [4] an algorithm controlling the MA input is presented for damping the high frequent vibrations of the suspension by using the additional sensor.

By using this control algorithm the remaining slow and large moving range of the VCM actuation can be used for positioning the head to the desired track with less negative effects of windage. One aspect to be avoided is the destructive effect of the two actuators by moving in opposite directions. A controller design technique taking this into account is the so called PQ control design method [5]. The PQ method allows the designer to work in the frequency domain and produces reasonable control designs for Dual Input Single Output (DISO) systems such as hard disk drives systems with dual stage actuators. Since there are two different bandwidth actuators, and so there exist restrictions to the working range of each actuator, a modification to the PQ method is made by explicitly considering the restrictions in the controller design. In this report it is presented that the modified PQ method will give good and acceptable results for the dual stage controller design.

In the next chapter the dual stage hard disk drive system is first discussed in more detail and in chapter 3 the modelling of the actuator and windage dynamics is discussed. In chapter 4 a schematic presentation of the control architecture is given and in chapter 5 the dual stage controller design by using the modified PQ method is presented. The results and analysis are given in chapter 6 and finally conclusions are drawn in chapter 7 and recommendations are given in chapter 8.

Chapter 2

System Description

Before discussing how to handle the control problem, the hard disk drive system will be discussed in more detail. First the dual stage suspension is discussed. The suspension consists of two stages. The first stage is driven by a VCM and the second stage is actuated by a MA. On the tip of the second stage is the read/write head attached. To provide the suspension with high frequent information it is instrumented with an additional sensor. The sensor as well as the MA is a strip made of a piezo-resistive material. Piezo-electric materials have the property that when it is polarized, it will expand or contract. This property is used to move and to measure the movements of the second stage of the suspension. The strips are both located between the first and second stage while the VCM is attached at the beginning of the first stage and moves the whole dual stage suspension compared to the case. From now on the first stage is defined as the base suspension and the second stage as the instrumented suspension. A schematic overview is given in figure 2.1.

To access data in different tracks located on the disk, position information is placed on the disk besides user data. The head is positioned with respect to this position information. Modern disk drives read the relative position of the head to the track directly from the disk media. This relative position is called a track mis-registration or an error in the position. In an experimental setup this position error can be measured by using a Laser Doppler Vibrometer (LDV). The LDV measurement results in a Position Error Signal (PES) and to limit the track mis-registration this PES needs to be bounded. This also requires the indirect measurement of the position error to be bounded. Therefore the signal coming from the additional sensor has to be minimized. This signal is called the Instrumented Suspension Signal (ISS) and can be obtained directly from the sensor.

To discuss a control problem it is necessary to describe how an input to a system can be observed in an output. For the hard disk drive system discussed in this report it means how the VCM input $u_{vcm}(t)$, the MA input $u_{ma}(t)$ and the windage induced disturbance can be observed in the PES $y_1(t)$ and ISS $y_2(t)$. Due to the discrete character of the measurements discrete time models are presented to describe these relations. The exact derivations of these models will be discussed in chapter 3.

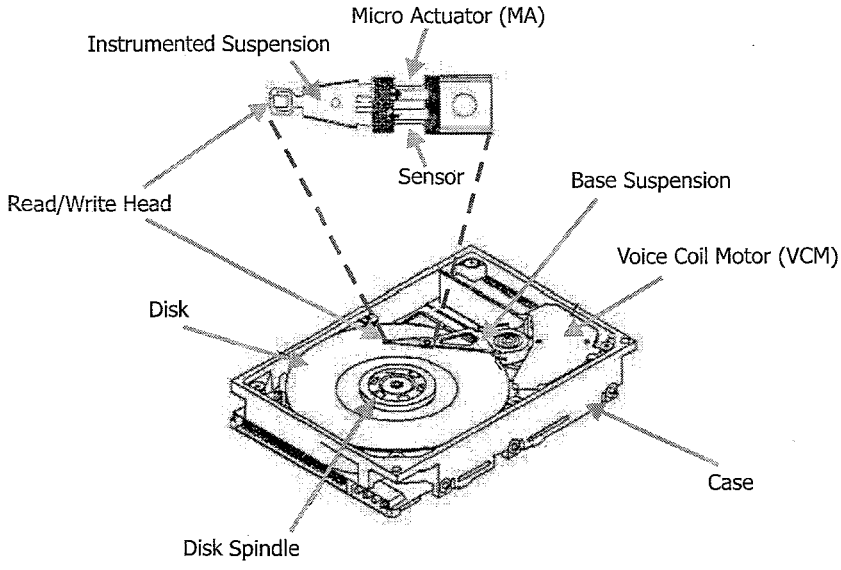

Figure 2.1: Schematic overview of a hard disk drive system with a dual stage instrumented suspension

The model $P_{vcm}(z)$ can be used to describe the relation between the VCM input $u_{vcm}(t)$ and the relative position of the head to disk $y_1(t)$. A discrete time model $P_{vcm}(z)$ is used because measurements of the relative position of the head to the disk are typically discrete time values due to the prescribed servo sectors on the disk. So the relationship is also described in discrete time where z is used as a short hand notation and denotes the shift operator with

$$z^{-1}x(t) = x(t-1) \tag{2.1}$$

and where $x(t)$ is a given signal in time. Further the relation between the MA input $u_{ma}(t)$ and the output $y_1(t)$ can be denoted by the discrete time model $P_{ma}(z)$ and a third model $P_i(z)$ can be used to describe the relation between the MA input $u_{ma}(t)$ and the output $y_2(t)$. From now on $P_{vcm}(z)$ is called the VCM dynamics, $P_{ma}(z)$ the MA dynamics and $P_i(z)$ the instrumented suspension dynamics.

To discuss the windage problem also the windage influence needs to be characterized. First let $d_1(t)$ be an additive term on $y_1(t)$ describing the windage induced disturbance acting on the PES. The stochastic properties of $d_1(t)$ can be characterized by a filtering

$$d_1(t) = H_{ma}(z)e(t) \tag{2.2}$$

where $e(t)$ represents the non-repeatable nature of the windage induced disturbance by a discrete white noise with a mean value and variance of respectively

$$\begin{aligned} E\{e(t)\} &= 0 \\ E\{e^2(t)\} &= \lambda \end{aligned} \tag{2.3}$$

Discrete time model $H_{ma}(z)$ is a stable and invertible stable filter and is used to represent the spectral contents of the flow induced vibrations resulting in een PES. This disturbance model is called the MA windage dynamics. Now $y_1(t)$ can be described by

$$y_1(t) = P_{vcm}(z)u_{vcm}(t) + P_{ma}(z)u_{ma}(t) + H_{ma}(z)e(t) \tag{2.4}$$

The wind will also influence the ISS. The stochastic properties of the windage induced disturbance $d_2(t)$ contributed to $y_2(t)$ are characterized by a filtering

$$d_2(t) = H_i(z)e(t) \tag{2.5}$$

where $e(t)$ is a white noise with properties as mentioned in (2.3). The discrete time model $H_i(z)$ is called the instrumented suspension windage dynamics and is used to represent the spectral contents of the flow induced vibrations resulting in an ISS. Now $y_2(t)$ can be described by

$$y_2(t) = P_i(z)u_{ma}(t) + H_i(z)e(t) \tag{2.6}$$

An overview of all the interactions between inputs and outputs as described in (2.4) and (2.6) is given in the block diagram shown in figure 2.2. Because the presented discrete time models will form the basis of the controller design these models will be determined in the next chapter.

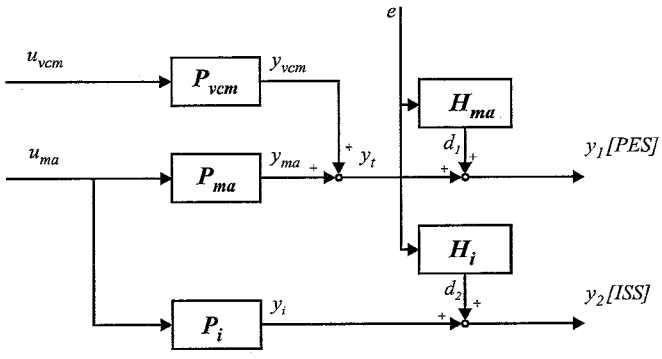

Figure 2.2: Block diagram of the hard disk drive system.

Chapter 3

Modelling

To formulate the input-output relations by the models mentioned in the previous chapter a standard Prediction Error (PE) estimation technique is used [6]. Using this technique models can be made out of experimental data. The PE estimation technique focused on characterizing the dynamics and the flow induced vibrations in a hard disk drive system is discussed before in [4] and [7]. In this report only a review of the PE estimation technique concerning the windage problem is given. Before going into detail about the hard disk drive system the modelling procedure is discussed considering a corresponding general system.

3.1 Modelling Procedure

Observing a causal dynamical system, with adequate freedom in describing the properties of a disturbance term, the input-output relationship can be expressed as

$$y(t) = f\big(u(t-1),\ ...,u(0),\ y(t-1),\ ...,\ y(0),\ e(t),\ ...,\ e(0)\big) \tag{3.1}$$

where $f(.)$ is a function modelling the system. Assuming the system is linear and time invariant and that the output only depends on a finite number of previous inputs and outputs, the input-output relationship can be expressed as a linear difference equation

$$\begin{aligned} y(t) + a_1 y(t-1) + ... + a_{n_a} y(t-n_a) = \\ b_1 u(t-1) + ... + b_{n_b} u(t-n_b) + e(t) + c_1 e(t-1) + ... + c_{n_c} e(t-n_c) \end{aligned} \tag{3.2}$$

where $y(t)$ represents the output and $u(t)$ represents the input of the system and with $e(t)$ representing the disturbance by a sequence of independent random variables with zero mean values and variances λ. The relation in (3.2) is the so called ARMAX model structure [6] and the adjustable parameters are is this case

$$\theta = [a_1\ a_2\ ...\ a_{n_a}\ b_1\ ...\ b_{n_b}\ c_1\ c_2\ ...\ c_{n_c}]^T \tag{3.3}$$

and has to be estimated to obtain the input-output relation.

Based on the information contained in N observations of the input and output data $\{u(t), y(t)\}$, $t = 0, ..., N$, discrete time models describing the input-output relation can be estimated. By introducing

$$\begin{aligned} A(z,\theta) &= 1 + a_1 z^{-1} + ... + a_{n_a} z^{-n_a} \\ B(z,\theta) &= b_1 z^{-1} + ... + b_{n_b} z^{-n_b} \\ C(z,\theta) &= 1 + c_1 z^{-1} + ... + c_{n_c} z^{-n_c} \end{aligned} \tag{3.4}$$

where z denotes the shift operator defined in (2.1), and defining

$$P(z,\theta) = \frac{B(z,\theta)}{A(z,\theta)} \tag{3.5}$$

$$H(z,\theta) = \frac{C(z,\theta)}{A(z,\theta)} \tag{3.6}$$

the input-output relation formulated in (3.2) can be rewritten in

$$y(t) = P(z,\theta)u(t) + H(z,\theta)e(t) \tag{3.7}$$

Here $P(z,\theta)$ and $H(z,\theta)$ are discrete time models describing the input-output relations. A schematic overview of this system with one input $u(t)$, one output $y(t)$ and one disturbance $e(t)$ is given in figure 3.1

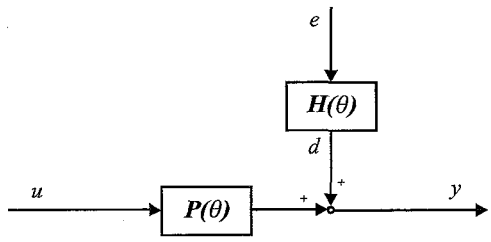

Figure 3.1: The ARMAX model structure

In the PE estimation technique the prediction of the output $y(t)$ on the basis of previous measurements $y(r), r = 0, ..., t-1$ is optimized. Considering measurements of input $u(t)$ and output $y(t)$, the one-step ahead prediction $y(t|t-1,\theta)$ of $y(t)$ is denoted by

$$y(t|t-1,\theta) = H(z,\theta)^{-1}P(z,\theta)u(t) + \left(1 - H(z,\theta)^{-1}\right)y(t) \tag{3.8}$$

This results in a prediction error given by

$$\varepsilon(t,\theta) = y(t) - y(t|t-1,\theta) \tag{3.9}$$

where $y(t)$ is the measured output of the system defined in (3.7). By minimizing the 2-norm of the prediction error the optimal parameter estimate can be determined. The optimal parameter estimate $\hat{\theta}$ is given by

$$\hat{\theta} = \min_{\theta} \left\| \varepsilon(t,\theta) \right\|_2 \tag{3.10}$$

and requires in general a non-linear optimization. Now the optimal models $P(z,\theta) := P(z,\hat{\theta})$ and $H(z,\theta) := H(z,\hat{\theta})$ can be found using the optimization in (3.10).

3.2 Identification of Actuator and Windage Dynamics

In this section the unknown input-output relations of the hard disk drive system with the windage induced disturbance, as described in (2.4) and (2.6), will be determined. By using the PE estimation technique discussed in section 3.1 the discrete time models $P_{vcm}(z)$, $P_{ma}(z)$, $P_i(z)$, $H_{ma}(z)$ and $H_i(z)$ can be estimated.

3.2.1 Experiments

The basis of estimating models for the hard disk drive system is given in (3.7). Here the models $P(z,\theta)$ and $H(z,\theta)$ can be estimated using the PE estimation technique based on one input $u(t)$ and one output $y(t)$ observation. Since the hard disk drive system has more inputs and outputs the estimation of the different models depends on the observed input and output. To obtain all the models three setups are presented

- Exciting $u_{vcm}(t)$ and observing $u_{vcm}(t)$ and $y_1(t)$ resulting in $P_{vcm}(z)$ and $H_{vcm}(z)$
- Exciting $u_{ma}(t)$ and observing $u_{ma}(t)$ and $y_1(t)$ resulting in $P_{ma}(z)$ and $H_{ma}(z)$
- Exciting $u_{ma}(t)$ and observing $u_{ma}(t)$ and $y_2(t)$ resulting in $P_i(z)$ and $H_i(z)$

Here $u_{vcm}(t)$ and $u_{ma}(t)$ are white noise signals exciting the system and are restricted to respectively ± 5 Volt and ± 10 Volt. For obtaining the PES $y_1(t)$ a LDV is used for non-contact measurements. Here 1 Volt from the LDV corresponds to a relative position of 4 μm between the head and the track on the disk. The ISS $y_2(t)$, in Volt, is obtained by using the additional sensor instrumented on the suspension.

The experimental data is obtained at the outer diameter of the disk and open-loop experiments are used to eliminate track following errors when the suspension is forced to follow a specific track on the disk. For the measurements a hard disk drive was used with a Hutchinson Magnum 5E suspension equipped with two piezo-resistive material strips for exciting the instrumented suspension and measuring the ISS. Inputs and outputs are observed during measurements over N=4096 data points with a sampling frequency of 40 kHz while the disk was rotating at a speed of 5400 rotations per minute.

3.2.2 Actuator and Windage Dynamics

To find the actuator and windage dynamics the model optimal parameters θ of $P_x(z,\theta)$ and $H_x(z,\theta)$ has to be optimized by minimizing the prediction error according to (3.9). Here x represents the three setups by respectively vcm, ma and i. Summarized the obtained models are

$$\{P_x(z,\theta), H_x(z,\theta)\}, \quad x = vcm, ma, i \tag{3.11}$$

The resulting models were used before in (2.4) and (2.6), except H_{vcm}. This disturbance model is supposed to be the same as H_{ma} because only one disturbance is acting on the suspension and results in a PES. Since the windage induced disturbance is a force disturbance on the suspension and will excite the modes of the suspension, the assumption is made that all the models of (3.11) will have identical resonance modes.

When using a state space representation as the parametrization of the models, the system matrix A will be the same for every model. Given the state space representation

$$\begin{aligned} \dot{x}(t) &= Ax(t) + Bu(t) \\ y(t) &= Cx(t) + Du(t) \end{aligned} \tag{3.12}$$

and considering (3.11) for $x = ma$ the parametrization for the MA dynamics and corresponding windage dynamics results in

$$P_{ma}(z,\theta) = C_1(zI - A)^{-1}B_1 + D_1 \tag{3.13}$$

$$H_{ma}(z,\theta) = C_1(zI - A)^{-1}B_2 + D_2 \tag{3.14}$$

Here the equivalent A and C_1 matrices denote the similar dynamical characteristics of the system model $P_{ma}(z,\theta)$ and disturbance model $H_{ma}(z,\theta)$ while measuring the PES. The different B and D matrices correspond to the different reference inputs $u_{ma}(t)$ and $e(t)$ respectively.

Considering the ISS measurement the system and disturbance model is given by

$$P_i(z,\theta) = C_2(zI - A)^{-1}B_3 + D_3 \tag{3.15}$$

$$H_i(z,\theta) = C_2(zI - A)^{-1}B_4 + D_4 \tag{3.16}$$

Again the A and C_2 matrices are equivalent for both models. Secondary the A matrix corresponds to the one used in (3.13) and (3.14) as expected. Also the different B and D matrices correspond to the different reference inputs $u_{ma}(t)$ and $e(t)$ respectively. Finally the VCM dynamics is obtained by measuring the PES and can be described by

$$P_{vcm}(z,\theta) = C_3(zI - A)^{-1}B_5 + D_5 \tag{3.17}$$

And again the A matrix is the same as is used in all the other models. The B_5 and D_5 matrices are obtained from inputs $u_{vcm}(t)$ and $e(t)$.

The get continuous time models to perform the control design in continuous time the discrete time models are converted to continuous time by using the zero-order hold method. More information about this can be found in chapters 4 and 5. The obtained system matrices of the 8th order state space models in continuous time are given in [4] and reviewed in appendix A. The A matrices presented are not similar for all models as stated before but the models are still describing the same dynamics because the state space models were balanced first. Bode diagrams are given in figures 3.2, 3.3 and 3.4. Now the identical resonance modes are apparent. To verify the obtained models also frequency responses of the three setups are measured. The measured and estimated frequency responses are given in appendix B.

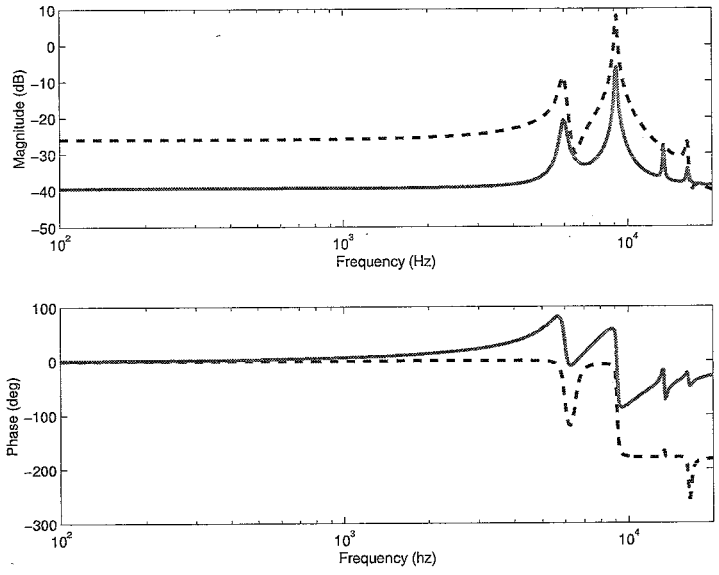

Figure 3.2: Bode diagram of P_{ma} (dashed) and H_{ma} (solid)

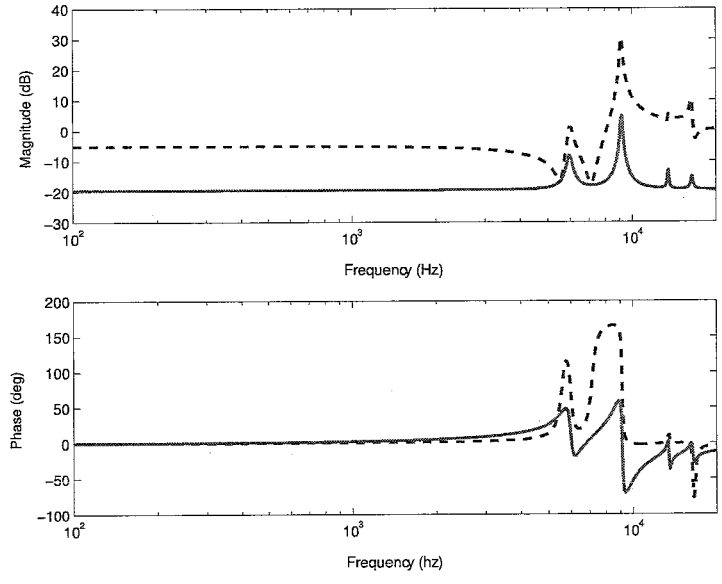

Figure 3.3: Bode diagram of P_i (dashed) and H_i (solid)

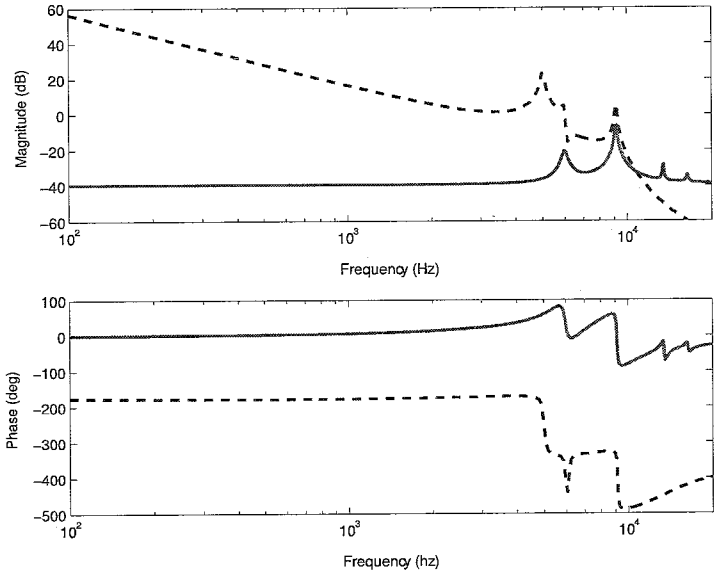

Figure 3.4: Bode diagram of P_{vcm} (dashed) and H_{ma} (solid)

Chapter 4

Control Architecture

The objective of disk drive control is to move the read/write head to the desired track as quickly as possible and to maintain it at the track as accurately as possible so that data can be transferred quickly and reliable. This means realizing a fast positioning and minimizing the track mis-registration. Considering the hard disk drive system with the windage induced disturbance, as given in figure 2.2, the two objectives can be accomplished by designing two controllers. A block diagram of the controlled hard disk drive system is given in figure 4.1.

First consider a controller for attenuating the high frequent vibrations. Attenuating these vibrations can be achieved by observing the ISS and controlling the MA input by a Single Input Single Output (SISO) feedback controller called the instrumented suspension controller C_i. Second consider a Single Input Dual Output (SIDO) controller measuring the PES and controlling the inputs u_{vcm} and u_{ma}. This controller is called the dual stage controller C_{ds} and needs be designed such that the closed loop system has a sufficient bandwidth for track following and seeking and attenuates the low frequent run out errors. Furthermore the limitation of the bandwidth of the VCM to the lower frequencies and the saturation limit of the MA at low frequencies should be taken into account in the controller design. A third aspect of the dual stage controller is to coordinate the movements of the two actuators. Because no independent measurements of y_{vcm} and y_{ma} are available destructive effects may occur when the VCM and MA are moving in opposite directions.

Because of the high sampling frequency of the ISS and because the MA is a fast responding mechanical system, controller C_i can be designed in continuous time. On the other hand the PES sampling frequency is limited to 20 kHz and in comparison to the high frequent resonance modes in the suspension, caused by the windage induced disturbance, discretization effects should be taken into account while designing C_{ds}. So C_{ds} has to be a discrete time controller and this makes the control design of a mixed continuous and discrete type.

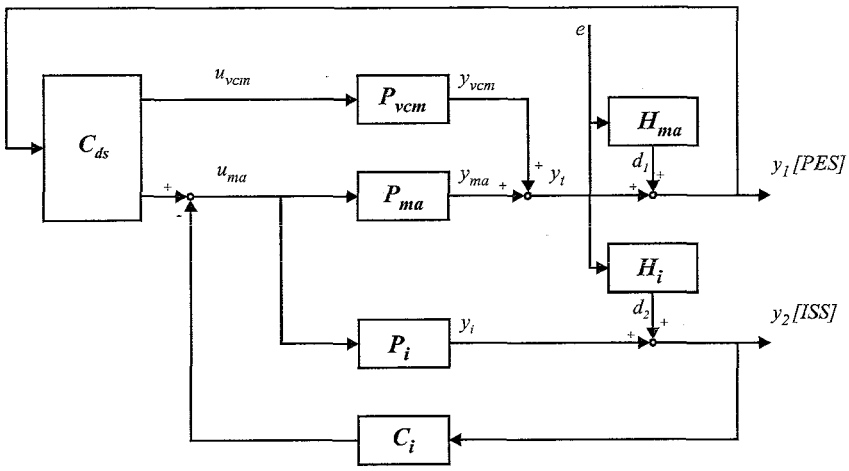

Figure 4.1: Block diagram of the controlled hard disk drive system.

4.1 General System Notation

Since the instrumented suspension controller is designed before [4] and the results will be used in the design of C_{ds}, the effectiveness of the high bandwidth control loop will be shown here. For this purpose two configurations of the control architecture are observed. Configuration A does not take the high bandwidth control loop with the ISS observation and C_i into account whereas configuration B does. To define the two configurations A and B a generalization of the controlled hard disk drive system is made. A block diagram is given in figure 4.2. Here E and F are introduced because the windage dynamics and system dynamics are different considering the two configurations. In configuration A the transfer functions for E and F in continuous time are given by

$$\begin{aligned} E(s) &= H_{ma}(s) \\ F(s) &= P_{ma}(s) \end{aligned} \tag{4.1}$$

where s is the Laplace parameter with $s \in \mathbb{C}$. Configuration B is the control architecture as given in figure 4.1. In appendix C this system is rewritten into the form of figure 4.2. The results for the transfer functions for E and F are given by respectively

$$\begin{aligned} E(s) &= H_{ma}(s) - \frac{P_{ma}(s)C_i(s)H_i(s)}{1 + C_i(s)P_i(s)} \\ F(s) &= \frac{P_{ma}(s)}{1 + C_i(s)P_i(s)} \end{aligned} \tag{4.2}$$

Bode diagrams of the disturbance model E and system model F in configuration A and B are given in appendix D. When comparing configuration A and B, the disturbance model in configuration B shows a clear attenuation (of about 20 dB) for the resonance peak at 9.1 kHz of configuration A. A consequence is that for the resonance peak at 6 kHz an amplification of 2 dB appears. In the bode diagram of system model F for configuration B also an amplification (of 12 dB) can be seen at 9.1 kHz.

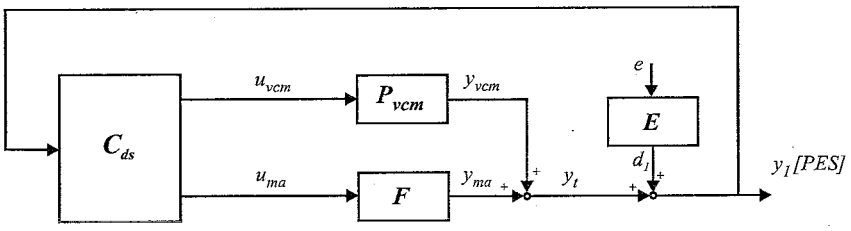

Figure 4.2: Generalization of the controlled hard disk drive system

It should be noted that this report presents the design of a dual stage controller for the dual stage instrumented suspension. For a more detailed discussion of the instrumented suspension controller C_i one is referred to [4]. From now on the controlled situation includes both the controllers C_{ds} and C_i, as is given in configuration B, and in the uncontrolled situation is no controller at all.

Chapter 5

Dual Stage Controller Design

To finish the control design the discrete time controller C_{ds} is discussed in this chapter. Considering the dual stage suspension, the VCM is used as an actuator for the first stage to generate a large but coarse and slow movement, while the MA is used as an actuator for the secondary stage to provide the fine a fast positioning. For the controller design of such dual stage actuators the PQ method can be used [5]. This frequency domain design technique transforms the SIDO controller design problem to two SISO design problems. Since the PQ method explicitly addresses the problem of destructive motion when two parallel actuators move in opposite directions it is appropriate to use here in stead of other design methods, like a master slave design technique or optimal control. A convenient representation of the dual stage controller using the PQ method is given in figure 5.1. Here controller C_{ds} consist of the three sub-controllers C_0, C_{vcm} and C_{ma}. The digital to analog (D/A) converters represent the discrete character of C_{ds} and the minus sign of C_0 represents the negative feedback.

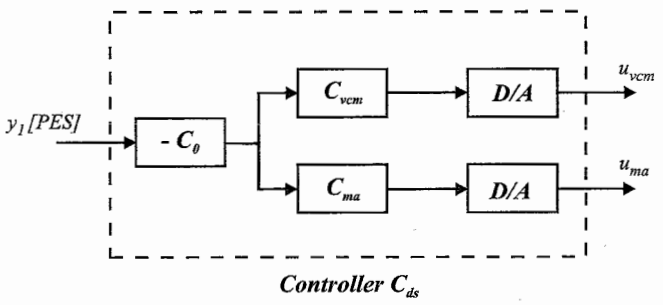

Figure 5.1: Representation of discrete time controller C_{ds} by using the PQ method

Since two control outputs are produced by a single PES measurement, controller C_{ds} can be subdivided into two parts. These two parts are a combination of $-C_0$ with C_{vcm} or C_{ma} and are defined by

$$\begin{aligned} C_{ds_{vcm}}(s) &= -C_0(s)C_{vcm}(s) \\ C_{ds_{ma}}(s) &= -C_0(s)C_{ma}(s) \end{aligned} \tag{5.1}$$

In section 5.1 the controller design is first performed into continuous time. The controller is designed in continuous time instead of the discrete time for simplicity reasons. This makes the iterative design procedure easier to understand. After the design in continuous time the controller is converted into discrete time in section 5.2. Finally in section 5.3 the dual stage controller results are presented.

5.1 Modified PQ Method in Continuous Time

In the PQ method the dual stage controller C_{ds} is designed in two steps. In the first step the frequency separation in working range between VCM and MA can be obtained and also movements of the VCM and MA in opposite directions can be prevented. The second step is for establishing the overall performance of the closed loop system given in figure 4.2. These two steps correspond to the two SISO control design problems. Now first the basis of transforming the SIDO control design problem to two SISO control design problems is discussed.

The first step is the design of a feedback controller Q for a SISO system P as given in figure 5.4. When considering the general system in figure 5.2, the transfer functions of P and Q are defined as respectively

$$P(s) = \frac{P_{vcm}(s)}{F(s)} \tag{5.2}$$

$$Q(s) = \frac{C_{vcm}(s)}{C_{ma}(s)} \tag{5.3}$$

Here P is the ratio of the two subsystems P_{vcm} and F and Q is the ratio of the controllers C_{vcm} and C_{ma}. The stability of the PQ feedback system can be determined by computing the location of the roots of its characteristic polynomial and whether they are all in the left half of the $\mathbb{C}$ plane. By using the definitions in (5.2) and (5.3), the characteristic polynomial of the PQ feedback system is given by

$$1 + Q(s)P(s) = \frac{C_{ma}(s)F(s) + C_{vcm}(s)P_{vcm}(s)}{C_{ma}(s)F(s)} \tag{5.4}$$

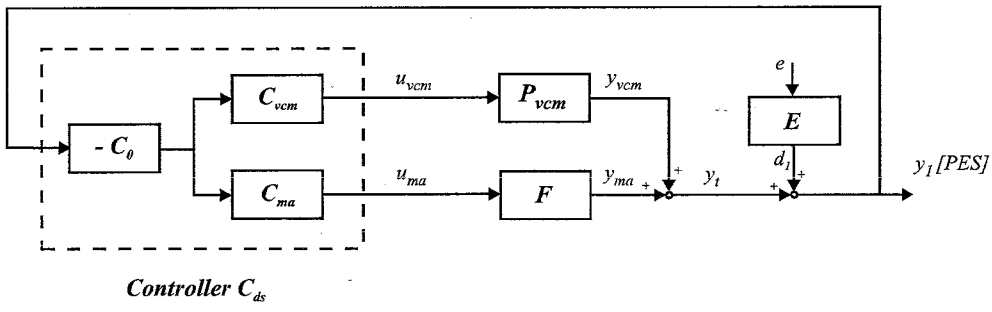

Figure 5.2: Generalization of the controlled hard disk drive system by using the PQ method in continuous time

Further the parallel combination of $C_{vcm}P_{vcm}$ and $C_{ma}F$ is considered. When observing figure 5.2, this parallel combination can be defined as a SISO system by introducing G_{siso}

$$G_{siso}(s) = C_{vcm}(s)P_{vcm}(s) + C_{ma}(s)F(s) \tag{5.5}$$

Using this definition for G_{siso} the characteristic polynomial of the PQ feedback system given in (5.4) results in

$$1 + Q(s)P(s) = \frac{G_{siso}(s)}{C_{ma}(s)F(s)} \tag{5.6}$$

Now the poles of the PQ feedback system corresponds to the zeros of $G_{siso}(s)$ and this relation forms the basis of the transformation of the SIDO design problem into two SISO design problems. So designing $Q(s)$ such that the PQ feedback system has stable poles ensures that $G_{siso}(s)$ has stable zeros according to (5.6). Stable zeros of $G_{siso}(s)$ are important since unstable zeros limit the stability and performance of the closed loop system given in figure 4.2. Finally the second step of the PQ method is a standard SISO design problem by designing controller C_0 for the system G_{siso} as given in the block diagram of figure 5.6.

5.1.1 Frequency Separation

Since the controller Q is the ratio of the two controllers C_{vcm} and C_{ma}, it can be used as an allocation of the relative contribution of the two parallel systems, $C_{vcm}P_{vcm}$ and $C_{ma}F$, to G_{siso}. By using the PQ method presented in literature [5] first controller Q has to be designed with explicit design freedom. Thereafter a selection has to be made for C_{vcm} and C_{ma} where C_{ma} is chosen to be one, and therefore C_{vcm} equals Q.

An other approach is first considering the limitations of the VCM and MA. With these limitations and with the stability requirements of the PQ feedback system, desired shapes of the transfer functions for C_{vcm} and C_{ma} can be given. Second by using (5.3) this results in a transfer function for controller Q. Now only the poles and zeros of controller Q have to be allocated to obtain the frequency separation. This approach will be used here and can be seen as a modification of the PQ method presented in literature.

Observing the VCM actuation the bandwidth is limited to the lower frequencies whereas the MA can only operate at higher frequencies due to saturation limits at the lower frequencies. Considering these limitations the desired transfer functions for C_{vcm} and C_{ma} will be like an integrator and differentiator respectively and are given by

$$\begin{aligned} C^*_{vcm}(s) &= \frac{\tau_d s + 1}{s} \\ C^*_{ma}(s) &= \frac{s}{\tau_d s + 1} \end{aligned} \tag{5.7}$$

Here τ_d is a time constant and the connection with the frequency domain is given by (5.8) for $x = d$. With f_x specifying a frequency operating as a break point, the time constant τ_x is defined as

$$\tau_x = \frac{1}{2\pi f_x} \tag{5.8}$$

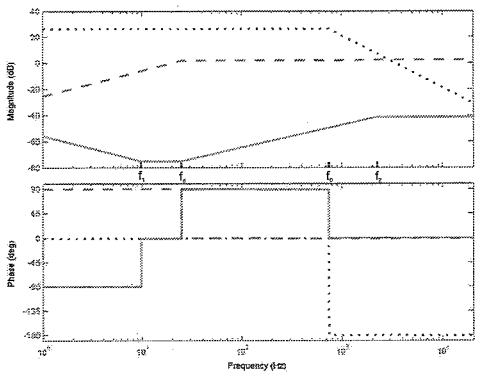

Figure 5.3: Bode diagram with asymptotes and breakpoints of controllers C_{vcm} (solid), C_{ma} (dashed) and C_0 (dotted)

In order to stabilize the PQ feedback system a lead compensator is added to the C_{vcm} and to adjust the gain of Q also a variable k is introduced. Now the transfer functions for C_{vcm} and C_{ma} are given by respectively

$$\begin{aligned} C_{vcm}(s) &= k\frac{\tau_d s+1}{s}\frac{\tau_1 s+1}{\tau_2 s+1} \\ C_{ma}(s) &= \frac{s}{\tau_d s+1} \end{aligned} \tag{5.9}$$

with $\tau_1 > \tau_2$ since a lead compensator is added. A bode diagram with asymptotes and breakpoints of the controllers C_{vcm} and C_{ma} is given in figure 5.3. The design freedom in Q for stabilizing the PQ feedback system is now modified into a given desired distribution of the control energy. With the definition in (5.3) controller Q results in

$$Q(s) = k\left(\frac{\tau_d s+1}{s}\right)^2 \frac{\tau_1 s+1}{\tau_2 s+1} \tag{5.10}$$

So designing Q for system P, as defined by respectively (5.10) and (5.2), ensures that the contribution to the response at the lower frequencies is dominated by the VCM actuation and at the higher frequencies the response is dominated by the MA actuation. At the 0-dB crossover frequency of open loop system PQ the contribution of the VCM and MA actuation is equal in

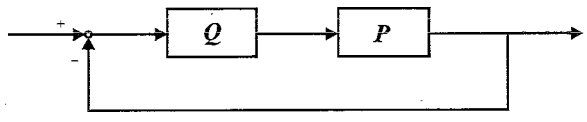

Figure 5.4: PQ feedback system

magnitude and destructive interference may occur. For a constructive motion of the two parallel systems the phase margin should be at least 60 degrees according to the PQ method [5].

For the hard disk drive system a bode diagram of transfer functions $P(s)$ and $P(s)Q(s)$ is given in figure 5.5. Here the phase margin of $P(s)Q(s)$ is 66 degrees at 489 Hz. This implies that the VCM and the MA dominates the motion respectively below and above this frequency and that at the 0-dB crossover frequency no interference occur. This will be demonstrated in chapter 6.

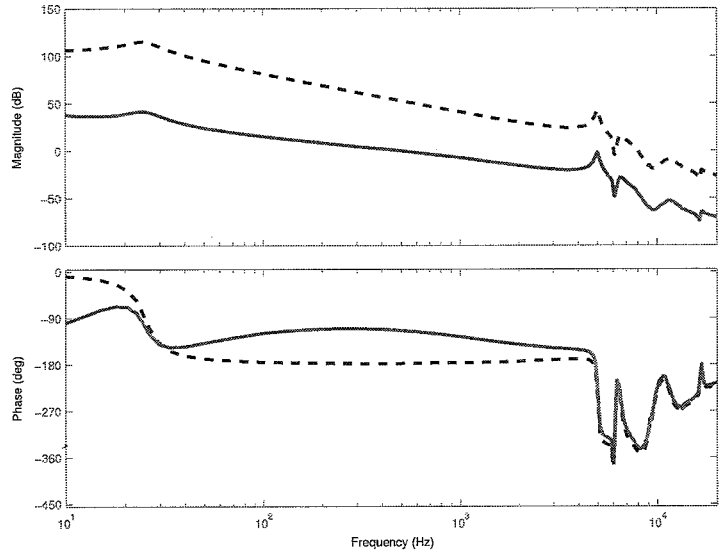

Figure 5.5: Bode diagram P (dashed) and PQ (solid)

5.1.2 Overall Performance

The second part of the PQ method consists of determining the overall performance for the closed loop system given in figure 4.2. This is a standard SISO design problem by designing controller C_0 for the system G_{siso}. A block diagram of the C_0G_{siso} feedback system is given in figure 5.6. To keep the controller as simple as possible and to obtain stability of the C_0G_{siso} feedback system, C_0 is proposed to be a second order low pass filter

$$C_0(s) = \frac{k_0}{\tau_0^2 s^2 + 2\beta_0\tau_0 s + 1} \tag{5.11}$$

with τ_0 a time constant and defined by (5.8) for $x = 0$, β_0 is the damping parameter and k_0 is an adjustable gain. In figure 5.3 the asymptotes and breakpoint of controller C_0 are given.

For the hard disk drive system bode diagrams of transfer functions $G_{siso}(s)$ and $C_0(s)G_{siso}(s)$ are given in figure 5.7. To fulfill stability and stability robustness requirements here C_0 is designed such that the maximum peak in de sensitivity function is maximum 6 dB. This will be

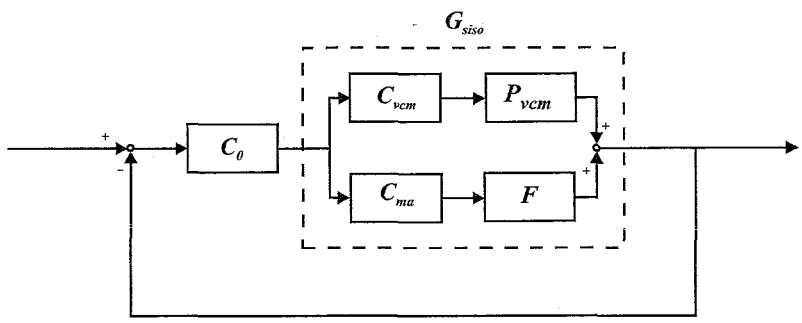

Figure 5.6: $C_0 G_{siso}$ feedback system

demonstrated in section 5.3. The corresponding gain margin is 10.9 dB at 8.9 kHz and the phase margin is 43.9 degrees at 687 Hz.

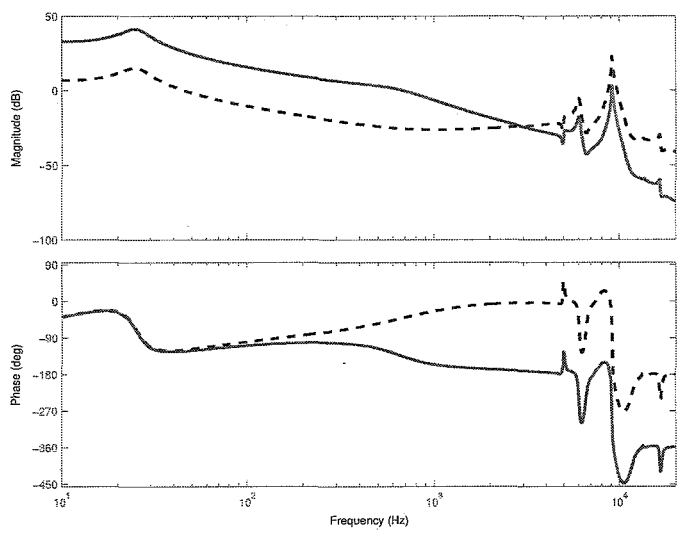

Figure 5.7: Bode diagram G_{siso} (dashed) and $C_0 G_{siso}$ (solid)

5.2 Conversion to Discrete Time Controller

The controller C_{ds} designed in the previous section is a continuous time controller based on continuous time system models. A general closed loop system in continuous time can be given as in figure 5.8(a). Since controller C_{ds} has to be implemented digitally side effects will occur because of the A/D and the D/A conversions of signals. In figure 5.8(b) the implemented closed loop of

figure 5.8(a) is given. Here the discrete time controller $C(z)$ is an approximation of the continuous time controller $C(s)$. The sampler is the A/D conversion representing the PES sampling with a sample period T and the zero-order hold (ZOH) is used as the D/A conversion. A ZOH holds each discrete value $u(kT)$ at the output of controller $C(z)$ constant until the next value, $u(kT+T)$, is available from the computer. Now the output of the ZOH $u(t)$, given in the implemented closed loop of figure 5.8(b), is a sequence of step functions and can be characterized in the $\mathcal{L}$aplace domain by transfer function

$$H_{ZOH}(s) = \frac{1-e^{-sT}}{s} \tag{5.12}$$

where T represents the sample period of the signals. So by implementation the ZOH adds destabilizing phase lag to the feedback loop. For evaluation of stability and performance of the closed loop system given in figure 5.8(b), a discrete equivalent closed loop system is given in figure 5.8(c). Here $P(s)$ is converted into discrete time by determining the ZOH equivalent. The closed loop combination of $P(z)$ and $C(z)$ exactly models $P(s)$ in the closed loop, as given in figure 5.8(a), at the sample times. For determining $P(z)$ a ZOH equivalent can be determined [8]. The ZOH equivalent of $P(s)$ is given by

$$P(z) = \mathcal{Z}\left\{\mathcal{L}^{-1}\left\{H_{ZOH}(s)P(s)\right\}\right\} \tag{5.13}$$

where $\mathcal{Z}$ and $\mathcal{L}^{-1}$ represents respectively the $\mathcal{Z}$-transform and the inverse $\mathcal{L}$aplace transform. This results for $P(z)$ in

$$P(z) = (1-z^{-1})\mathcal{Z}\left\{\mathcal{L}^{-1}\left\{\frac{P(s)}{s}\right\}\right\} \tag{5.14}$$

The foregoing was applied to a general closed loop system. Concerning the hard disk drive system the transformation of (5.14) has to be applied to system dynamics $P_{vcm}(s)$ and $F(s)$ because of the representation of the discrete dual stage controller given in figure 5.1.

For the approximation of controller $C(s)$ a bi-linear transformation like Tustin's method can be used to determine a discrete equivalent [8]. Given the continuous time transfer function $C(s)$, the discrete equivalent can be determined by the substitution

$$C(z) = C(s)\Big|_{s=\frac{2}{T}\frac{z-1}{z+1}} \tag{5.15}$$

where T is the sample period. For the dual stage controller C_{ds} designed in the previous section the discrete equivalents of (5.1) are given by respectively

$$\begin{aligned} C_{ds_{vcm}}(z) &= -C_0(z)C_{vcm}(z) \\ C_{ds_{ma}}(z) &= -C_0(z)C_{ma}(z) \end{aligned} \tag{5.16}$$

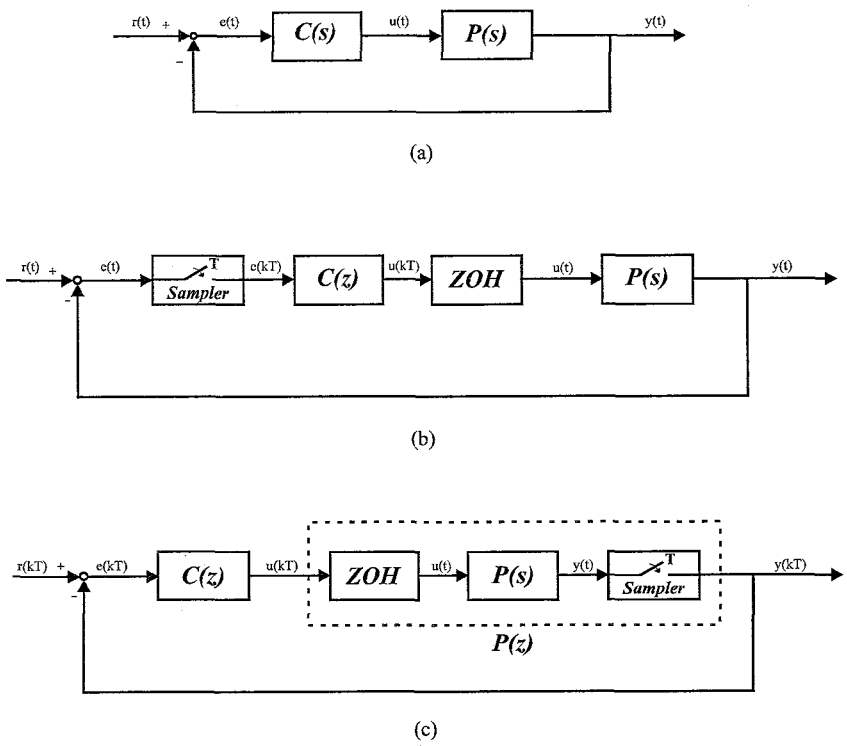

Figure 5.8: (a) Closed loop system in continuous time. (b) Implemented closed loop system. (c) Stability and performance evaluation of the closed loop system given in (b).

To determine the discrete time controllers $C_{vcm}(z)$, $C_{ma}(z)$ and $C_0(z)$ the substitution given in (5.15) has to be used. This results in respectively

$$C_{vcm}(z) = k\frac{\big((2\tau_d + T)z - (2\tau_d - T)\big)}{2(z-1)}\frac{\big((2\tau_1 + T)z - (2\tau_1 - T)\big)}{\big((2\tau_2 + T)z - (2\tau_2 - T)\big)}$$

$$C_{ma}(z) = \frac{2(z-1)}{(2\tau_d + T)z - (2\tau_d - T)} \tag{5.17}$$

$$C_0(z) = \frac{k_0 T^2 (z+1)^2}{(4\tau_0^2 + 4\beta_0\tau_0 T + T^2)z^2 - (8\tau_0^2 - 2T^2)z + (4\tau_0^2 - 4\beta_0\tau_0 T + T^2)}$$

When determining a discrete equivalent a cut-off frequency occur at half the sample frequency, also called the Nyquist frequency. In the case the discrete equivalence is determined by Tustin's method the practical cut-off frequency occurs already before the Nyquist frequency. Observing the hard disk drive system with a PES sample frequency of 20 kHz, the consequences for both

parallel systems, $C_{vcm}P_{vcm}$ and $C_{ma}F$, are an attenuation of the resonance peak at 9.1 kHz. Therefore also the resonance peak at 9.1 kHz of G_{siso} is attenuated. Now this attenuation of G_{siso} creates new design freedom for C_0 in increasing the bandwidth of the system. But since in the windage disturbance model a resonance peak occurs at 6 kHz, which does not want to be amplified, a compromise has to be found in increasing the bandwidth. The fact is that increasing the bandwidth of the system gives a disturbance reduction below the bandwidth, but according to Bode's sensitivity integral this is at the cost of disturbance amplification at high frequencies. Now C_0 is redesigned under the condition that the negative influence on the windage disturbance is as small as possible and again, to fulfill stability and stability robustness requirements, C_0 is redesigned such that the maximum peak in de sensitivity function is maximum 6 dB. The new Bode diagram of the open loop system C_0G_{siso} is given in figure 5.9. The corresponding gain margin is 9.9 dB at 3.70 kHz and the phase margin is 68.9 degrees at 1.7 kHz.

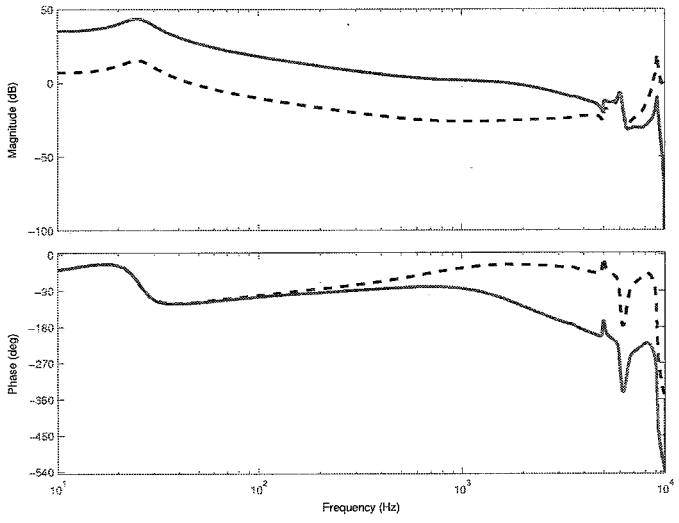

Figure 5.9: Bode diagram G_{siso} (dashed) and C_0G_{siso} (solid) in discrete time

5.3 Controller Results

The results of the stable dual stage controller C_{ds} are presented here. The control parameters are given in table 5.1 for the continuous time controller, as given in (5.1), as well as for the discrete time controller, as given in (5.16). The corresponding bode diagrams are given in figure 5.10.

Table 5.1: Control parameters and degree of stability for continuous and discrete time domain

Time Domain	k	k_0	τ_d	τ_0	τ_1	τ_2	β_0	GM	PM
	[-]	[-]	[ms]	[ms]	[ms]	[ms]	[-]	[dB]	[deg]
Continuous	1.001	20	9.091	0.244	9.091	0.118	0.5	10.9	37.7
Discrete	1.001	26	9.091	9.091	9.091	0.118	0.7	9.9	68.9

The stability and stability robustness requirements for the closed loop system, as given in figure 4.2, can be analyzed using the Nyquist diagram of the open loop system C_0G_{siso}. This diagram is given in figure 5.11. The Nyquist diagram of the open loop system can be used to check the stability of the closed loop system since the poles of the closed loop system correspond to the point -1. For point -1 in the Nyquist diagram of the open loop system, the phase shift is -180 degrees and the magnitude is 1. For stability it is important to stay away from this point. When

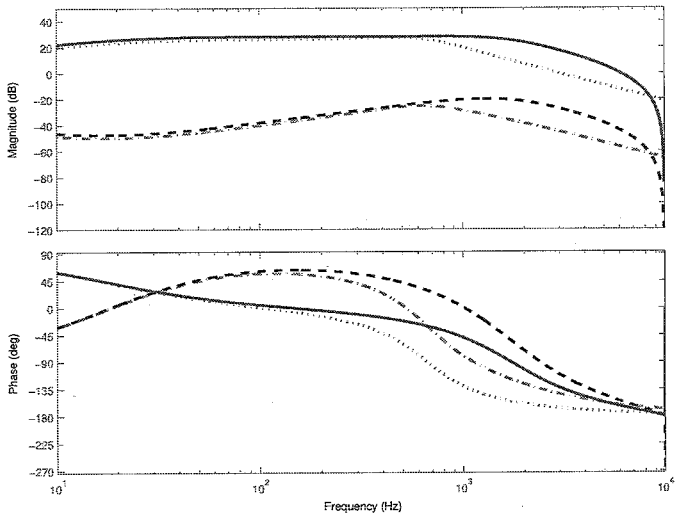

Figure 5.10: Discrete time controller $C_{ds_{vcm}}$ (dashed) and $C_{ds_{ma}}$ (solid) and continuous time controller $C_{ds_{vcm}}$ (dash-dotted) and $C_{ds_{ma}}$ (dotted)

the phase shift is -180 degrees the magnitude has to smaller than one or when the magnitude is 1 the phase shift has to be less than -180 degrees. To check stability and stability robustness requirements in the Nyquist diagram, also a contour is given for the sensitivity function as shown in figure 5.11. This contour shows the magnitude at which the sensitivity function (S) is 6 dB. For the hard disk drive system the corresponding degree of stability is given by the Gain Margin (GM) and Phase Margin (PM) in table 5.1.

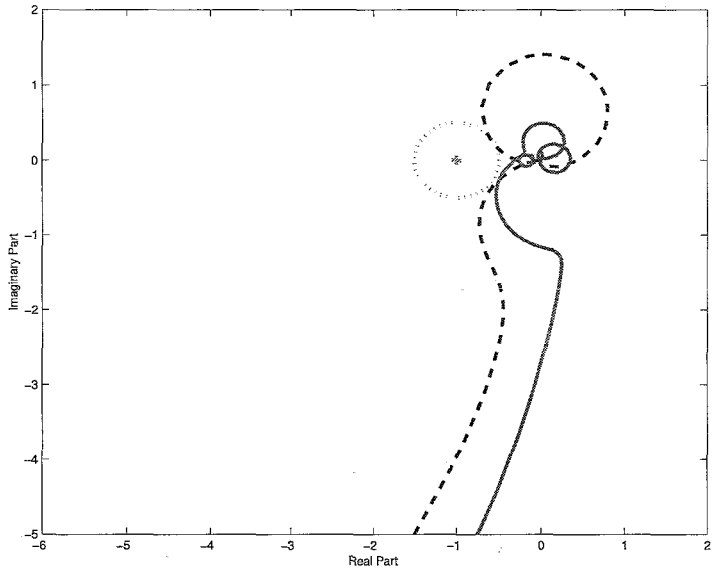

Figure 5.11: Nyquist diagram of the open loop system $C_0 G_{siso}$ in discrete time (solid) and in continuous time (dashed) and with $|S| = 6$ dB (dotted)

Chapter 6

Closed Loop Results and Analysis

In this chapter the results of the discrete dual stage controller design for the closed loop system will be given. In the first section the frequency separation as proposed by the modified PQ method is discussed. In section 6.2 the disturbance reduction obtained by the dual stage controller as well the instrumented suspension controller is presented.

6.1 Frequency Separation

In the design of controller C_{ds} the modified PQ method was used to obtain a frequency separation

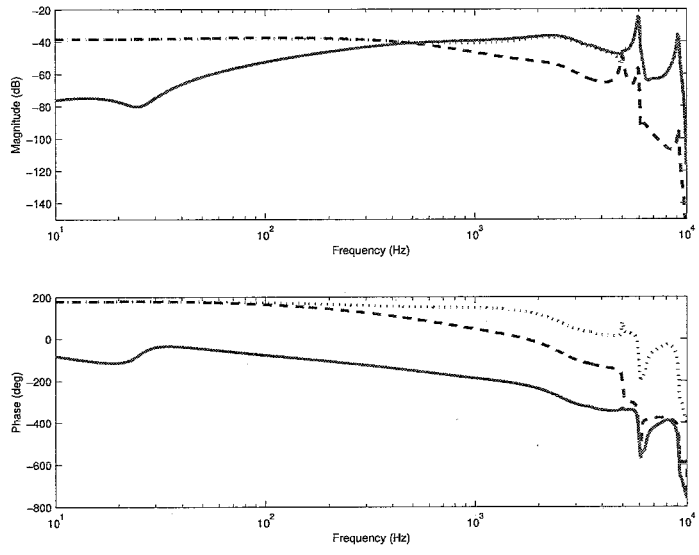

Figure 6.1: Bode diagram of the contribution of y_{vcm} (dashed) and y_{ma} (solid) to y_t (dotted)

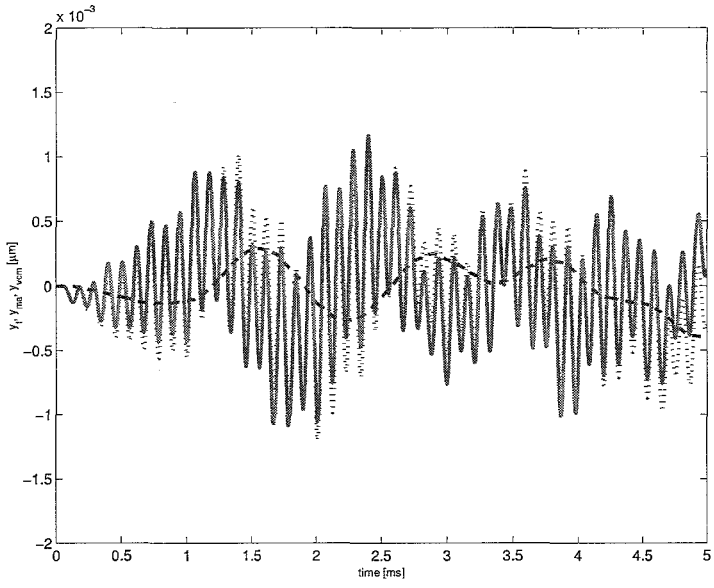

Figure 6.2: Time response of the contribution of y_{vcm} (dashed) and y_{ma} (solid) to y_t (dotted)

in the working range of the two parallel subsystems. This was necessary since there were two actuators with different bandwidths. In figure 6.1 the contribution of the output of the subsystems to y_t are given as function of the frequency. This figure makes clear that at the lower frequencies the response of y_t is dominated by the VCM actuator whereas at the higher frequencies the MA dominates. This is expected since in the modified PQ method the transfer functions for C_{vcm} and C_{ma} were selected according to these results.

The separation frequency in working range at 489 Hz was obtained by selecting the 0-dB crossover frequency of the PQ feedback system. In figure 6.1 the phase of y_{vcm} and y_{ma} at this frequency is respectively -162 degrees and 84 degrees. This gives a phase difference between y_{vcm} and y_{ma} of 246 degrees or $360 - 246 = 114$ degrees. According to the theory as stated in the the PQ method [5] the phase margin of the open loop PQ should be $180 - 114 = 66$ degrees. Indeed this exactly equals the selected phase margin of the open loop PQ for the hard disk drive system.

The obtained frequency separation can also be demonstrated in the time domain. The responses y_{vcm}, y_{ma} and y_t are simulated in the case a windage disturbance is acting on the system. The results are given in figure 6.2. It can be seen that the reaction of MA on a windage disturbance is much heavier than the VCM reaction. This also becomes clear when observing the inputs to VCM and MA as given in appendix E. The MA utilizes its maximum input range (± 10 Volt) whereas the VCM utilizes only a few percent of its capacity (± 5 Volt).

One other aspect that can be seen in the simulation results of figure 6.2 is the constructive motion of the two subsystems. There is still a phase difference between y_{vcm} and y_{ma} but in fact we have selected a relatively small phase margin. If a fully constructive motion is desired a phase margin of 180 degrees should be selected. Also from a physical point of view the phase lag is expected. This because the MA is a faster responding system that the VCM.

6.2 Disturbance Reduction

The attenuation of the high frequent windage vibration by the high bandwidth control loop was already discussed and presented in section 4.1. For analyzing the disturbance reduction obtained by the dual stage controller the closed loop system, as given in figure 4.2 for configuration B, is observed. This disturbance reduction is necessary for track following since there exist low frequent run out errors. The sensitivity function of this closed loop system is given by

$$\begin{aligned} S(z) &= \frac{1}{1 + C_0(z)G_{siso}(z)} \\ &= \frac{1}{1 + C_0(z)C_{vcm}(z)P_{vcm}(z) + C_0(z)C_{ma}(z)F(z)} \end{aligned} \tag{6.1}$$

This sensitivity function gives the disturbance reduction obtained by the combined subsystems. The disturbance reduction obtained by only controlling the VCM input is given by

$$S_{vcm}(z) = \frac{1}{1 + C_0(z)C_{vcm}(z)P_{vcm}(z)} \tag{6.2}$$

With this sensitivity function of only the VCM actuation the overall sensitivity function S, as given in (6.1), can be rewritten into

$$S(z) = S_{vcm}(z)S_{ma}(z) \tag{6.3}$$

Here S_{ma} gives the contribution of the MA to the overall disturbance reduction and so the improvement on the disturbance reduction obtained by only the VCM actuation.

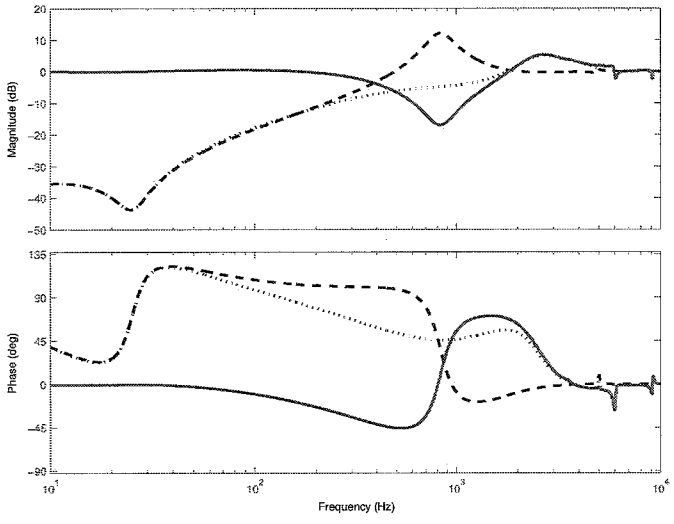

Figure 6.3: Closed loop sensitivity functions S (dotted), S_{vcm} (dashed) and S_{ma} (solid)

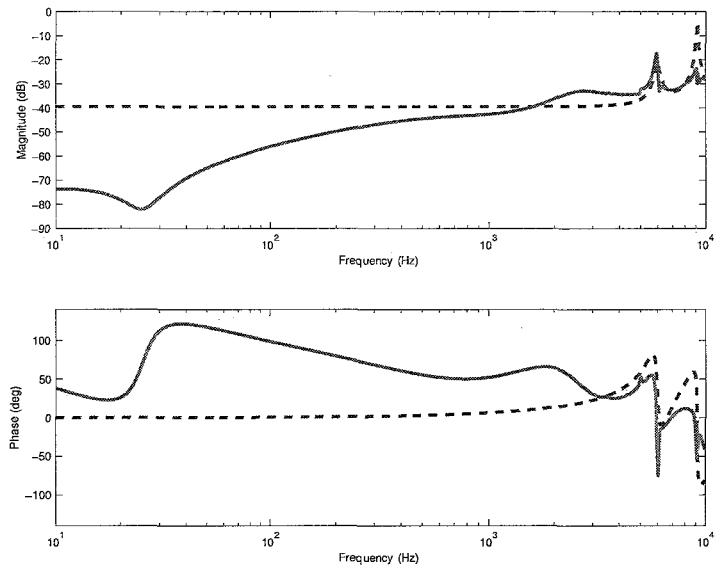

Figure 6.4: Bode diagram of the disturbance reduction without (dashed) and with control (solid)

With the derivation of (6.3) given in appendix C.4, S_{ma} is defined by

$$\begin{aligned} S_{ma} &= 1 - C_0(z)C_{ma}(z)F(z)S(z) \\ &= \frac{1}{1 + C_0(z)C_{ma}(z)F(z)S_{vcm}(z)} \end{aligned} \tag{6.4}$$

Now when observing S_{ma} directly the improvement on S_{vcm} can be seen. In figure 6.3 the bode diagrams of S_{ma}, S_{vcm} and S are given. For the lower frequencies the disturbance reduction is obtained by the VCM till a frequency of 489 Hz as is given by S_{vcm}. Observing S_{ma}, an additional disturbance reduction on S_{vcm} between 170 Hz and 1.7 kHz is obtained. This results in a total disturbance reduction till a frequency of 1.7 kHz as is given by S. On the other hand in the frequency range of 1.7 kHz to 5.9 kHz in the bode diagram of S there exists an amplification. This amplification is directly a consequence of the Bode's sensitivity integral property as discussed in section 5.2. In this section a compromise was made in the design of controller C_0 concerning the bandwidth and the amplification of the resonance peak at 6 kHz of the disturbance model.

The final disturbance reduction becomes clear when observing the closed loop disturbance model. For the closed loop system with the dual stage controller the disturbance model is given by

$$H(z) = E(z)S(z) \tag{6.5}$$

Here $E(z)$ is the discrete equivalent of the disturbance model $E(s)$ as was discussed in section 4.1. Now the control architecture of configuration B is considered and so both the controllers C_i and C_{ds} are taken into account. In figure 6.4 the new disturbance model H is compared to the original uncontrolled disturbance model H_{ma}. Here again the low frequent disturbance reduction can be seen, but the consequence of the dual stage controller is that an amplification of 3 dB of the resonance peak at 6 kHz is involved.

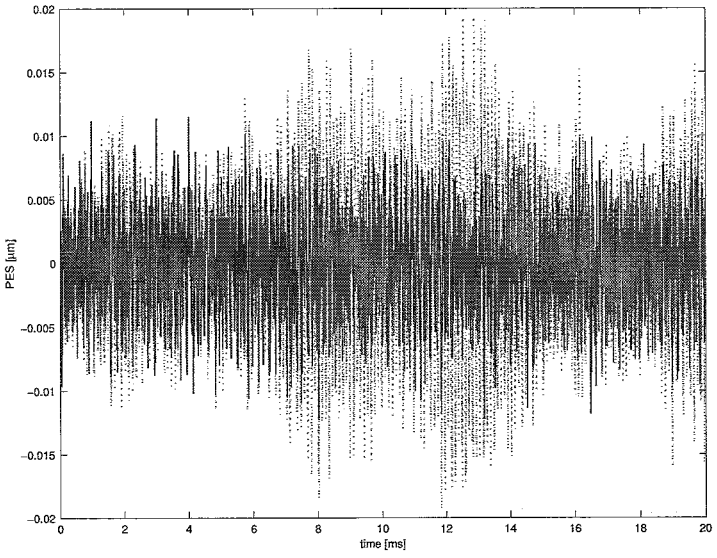

Figure 6.5: Time response of the simulation of the PES without (dashed) and with control (solid)

The improvement of both the controllers C_i and C_{ds} on the disturbance reduction can also be found in the time response of the PES as is shown in figure 6.5. For the improvement the energy ratio in de controlled and uncontrolled situation can be observed. This energy ratio is given by the ratio of the squared 2-norm of the PES output.

$$\frac{\left\| y_{1_{controlled}} \right\|_2^2}{\left\| y_{1_{uncontrolled}} \right\|_2^2} = 0.48 \tag{6.6}$$

This ratio means an improvement on the PES of 48 percent when using control.

Chapter 7

Conclusions

In a hard disk drive system with a dual stage instrumented suspension and a large windage disturbance a dual stage controller was designed by using the modified PQ method. Therefore first a description of the system with the windage disturbance was made and models describing the system and windage dynamics were given. Second the control problem was discussed. Because of the large and high frequent windage disturbance two controllers were suggested. For attenuating the windage disturbance a high bandwidth controller already existed. The second controller was the dual stage controller. This controller was designed under the condition that the negative influence on the windage disturbance was small and with the stability requirement of a maximum peak in de sensitivity function of maximum 6 dB. This has resulted in a control loop with a bandwidth of 1.7 kHz and a gain and phase margin of respectively 9.9 dB and 68.9 degrees.

Since the dual stage instrumented suspension contained two different bandwidth actuators, a frequency separation in the output contribution of the two actuators was desired. To obtain the frequency separation the modified PQ method was introduced for the controller design. The modified PQ method is a modification of the PQ method and in stead of the PQ method the modified PQ method explicitly considers the bandwidth limitations of the two actuators. This has resulted in a separation frequency at 489 Hz and this frequency corresponds to the 0-dB crossover frequency of the PQ feedback system. To prevent the two actuators also moving in opposite directions when the output contribution is equal, a phase margin for the PQ feedback system was selected to be 66 degrees. The selected frequency separation frequency as well as the selected phase margin were also shown in the closed loop results. Finally together with the high bandwidth controller an improvement on the PES of 48 percent was obtained.

Chapter 8

Recommendations

When observing the closed loop disturbance model the resonance peak at 6 kHz dominates the disturbance in stead of the resonance peak at 9.1 kHz. This is directly a consequence of the high bandwidth controller as well as the dual stage controller. The high bandwidth controller was mainly designed to attenuate the resonance peak at 9.1 kHz in stead of the resonance peak at 6 kHz and when the dual stage controller was designed a compromise was found in increasing the bandwidth and affecting the windage disturbance. Since it is desirable to have both resonance modes, at 6 kHz and at 9.1 kHz, as small as possible in magnitude, it is recommended to redesign the high bandwidth controller. In the new design of this controller more attention should be paid to the resonance mode at 6 kHz.

Further in this report it is only shown that the modified PQ method give good and acceptable results for the dual stage controller design. However it is possible that the original PQ method or other design methods, like a master slave design method or optimal control, give better results. Therefore, when interested in the best result, it is recommended to compare the modified PQ method for dual stage controller design to the controller results obtained from other methods.

Appendix A

System State Space Models

A.1 VCM Dynamics P_{vcm}

$$A = \begin{bmatrix} -20.253 & 156.58 & -3.8316 & -3.067 & 1.3841 & -0.69702 & 1.1927 & -1.1352 \\ -156.58 & -27.248 & 5.1562 & 4.1346 & -1.8646 & 0.93869 & -1.6066 & 1.5289 \\ 3.8316 & 5.1562 & -471.9 & -31432 & 404.02 & -148.74 & 329.77 & -252.81 \\ -3.067 & -4.1346 & 31432 & -310.27 & 241.43 & -167.52 & 217.05 & -257.69 \\ 1.3841 & 1.8646 & -404.02 & 241.43 & -395.67 & 57454 & -401.55 & 2048.4 \\ 0.69702 & 0.93869 & -148.74 & 167.52 & -57454 & -101.01 & 1164.1 & -194.94 \\ 1.1927 & 1.6066 & -329.77 & 217.05 & -401.55 & -1164.1 & -420.82 & 37409 \\ 1.1352 & 1.5289 & -252.81 & 257.69 & -2048.4 & -194.94 & -37409 & -389.5 \end{bmatrix}$$

$$B = \begin{bmatrix} -885.34 \\ -884.35 \\ 83.716 \\ -67.06 \\ 30.255 \\ 15.234 \\ 26.07 \\ 24.811 \end{bmatrix}$$

$$C = \begin{bmatrix} -885.34 & 884.35 & -83.716 & -67.06 & 30.255 & -15.234 & 26.07 & -24.811 \end{bmatrix}$$

$$D = \begin{bmatrix} 0 \end{bmatrix}$$

A.2 MA Dynamics P_{ma}

$$A = \begin{bmatrix} -318.72 & 57439 & -315.53 & 326.61 & -135.28 & 103.18 & -89.115 & 37.48 \\ -57417 & -343.81 & 409.43 & -281.28 & 138.2 & -110.22 & 93.569 & -38.631 \\ -308.98 & -403.87 & -875.82 & 37596 & -748.72 & 473.9 & -440.23 & 199.15 \\ -281.1 & -272.67 & -37534 & -658.55 & 534.42 & -517.65 & 396.7 & -159.34 \\ 120.05 & 137.23 & 721.38 & 530.68 & -1200 & 1.0268 \cdot 10^5 & -3346.2 & 779.39 \\ 97.246 & 110.17 & 466.98 & 504.34 & -1.0267 \cdot 10^5 & -741.81 & 2371.7 & -1677.8 \\ -42.969 & -14.126 & -110.53 & 0.068398 & 2435.4 & -1508.4 & -749.25 & 84868 \\ -33.785 & -26.216 & -165.42 & -70.601 & -158.37 & 1587.2 & -84812 & -130.38 \end{bmatrix}$$

$$B = \begin{bmatrix} 31.441 \\ 33.047 \\ 17.677 \\ 14.088 \\ -6.5658 \\ -5.2548 \\ 1.2515 \\ 1.4629 \end{bmatrix}$$

$$C = \begin{bmatrix} 32.29 & -33.358 & 17.697 & -15.051 & 6.7831 & -5.2847 & 4.5334 & -1.8848 \end{bmatrix}$$

$$D = \begin{bmatrix} 0 \end{bmatrix}$$

A.3 MA Windage Dynamics H_{ma}

$$A = \begin{bmatrix} -318.72 & 57439 & -315.53 & 326.61 & -135.28 & 103.18 & -89.115 & 37.48 \\ -57417 & -343.81 & 409.43 & -281.28 & 138.2 & -110.22 & 93.569 & -38.631 \\ -308.98 & -403.87 & -875.82 & 37596 & -748.72 & 473.9 & -440.23 & 199.15 \\ -281.1 & -272.67 & -37534 & -658.55 & 534.42 & -517.65 & 396.7 & -159.34 \\ 120.05 & 137.23 & 721.38 & 530.68 & -1200 & 1.0268 \cdot 10^5 & -3346.2 & 779.39 \\ 97.246 & 110.17 & 466.98 & 504.34 & -1.0267 \cdot 10^5 & -741.81 & 2371.7 & -1677.8 \\ -42.969 & -14.126 & -110.53 & 0.068398 & 2435.4 & -1508.4 & -749.25 & 84868 \\ -33.785 & -26.216 & -165.42 & -70.601 & -158.37 & 1587.2 & -84812 & -130.38 \end{bmatrix}$$

$$B = \begin{bmatrix} 7.3869 \\ -4.5406 \\ 0.84395 \\ -5.2979 \\ 1.7030 \\ 0.56085 \\ 4.3572 \\ 1.1883 \end{bmatrix}$$

$$C = \begin{bmatrix} 32.29 & -33.358 & 17.697 & -15.051 & 6.7831 & -5.2847 & 4.5334 & -1.8848 \end{bmatrix}$$

$$D = \begin{bmatrix} 0.010632 \end{bmatrix}$$

A.4 Instrumented Suspension Dynamics P_i

$$A = \begin{bmatrix} -293.21 & 57429 & -318.14 & 218.72 & -161.05 & 152.63 & 69.948 & 87.78 \\ -57427 & -366.97 & 314.96 & -279.09 & 191.49 & -163.28 & -80.535 & -96.458 \\ 316.89 & 314.94 & -1188.6 & 1.0292 \cdot 10^5 & -2330.7 & 865.82 & 689.51 & 584.08 \\ 218.43 & 278.72 & -1.0292 \cdot 10^5 & -736.25 & 732.57 & -1617.8 & -380.34 & -677.96 \\ -160.12 & -187.58 & 2312.7 & 710.57 & -839.38 & 37655 & 505.77 & 1517.9 \\ -140.67 & -155.33 & 765.36 & 1575.3 & -37556 & -705.57 & -1138.4 & -574.33 \\ 67.277 & 74.984 & -657.64 & -351.65 & 487.49 & 1034.7 & -352.83 & -84587 \\ -85.217 & -95.475 & 574.43 & 669.09 & -1480.7 & -554.38 & 84530 & -535.5 \end{bmatrix}$$

$$B = \begin{bmatrix} -108.81 \\ -121.11 \\ 55.342 \\ 43.191 \\ -30.36 \\ -25.976 \\ 12.436 \\ -15.842 \end{bmatrix}$$

$$C = \begin{bmatrix} 108.99 & -121.24 & 55.38 & -43.193 & 30.761 & -27.668 & -13.152 & -16.125 \end{bmatrix}$$

$$D = \begin{bmatrix} 1.0216 \end{bmatrix}$$

A.5 Instrumented Suspension Windage Dynamics H_i

$$A = \begin{bmatrix} -293.21 & 57429 & -318.14 & 218.72 & -161.05 & 152.63 & 69.948 & 87.78 \\ -57427 & -366.97 & 314.96 & -279.09 & 191.49 & -163.28 & -80.535 & -96.458 \\ 316.89 & 314.94 & -1188.6 & 1.0292 \cdot 10^5 & -2330.7 & 865.82 & 689.51 & 584.08 \\ 218.43 & 278.72 & -1.0292 \cdot 10^5 & -736.25 & 732.57 & -1617.8 & -380.34 & -677.96 \\ -160.12 & -187.58 & 2312.7 & 710.57 & -839.38 & 37655 & 505.77 & 1517.9 \\ -140.67 & -155.33 & 765.36 & 1575.3 & -37556 & -705.57 & -1138.4 & -574.33 \\ 67.277 & 74.984 & -657.64 & -351.65 & 487.49 & 1034.7 & -352.83 & -84587 \\ -85.217 & -95.475 & 574.43 & 669.09 & -1480.7 & -554.38 & 84530 & -535.5 \end{bmatrix}$$

$$B = \begin{bmatrix} 6.2653 \\ -5.6308 \\ 2.0538 \\ -0.38126 \\ 4.9497 \\ -9.5266 \\ -4.2804 \\ -3.0079 \end{bmatrix}$$

$$C = \begin{bmatrix} 108.99 & -121.24 & 55.38 & -43.193 & 30.761 & -27.668 & -13.152 & -16.125 \end{bmatrix}$$

$$D = \begin{bmatrix} 0.10632 \end{bmatrix}$$

Appendix B

System Frequency Responses

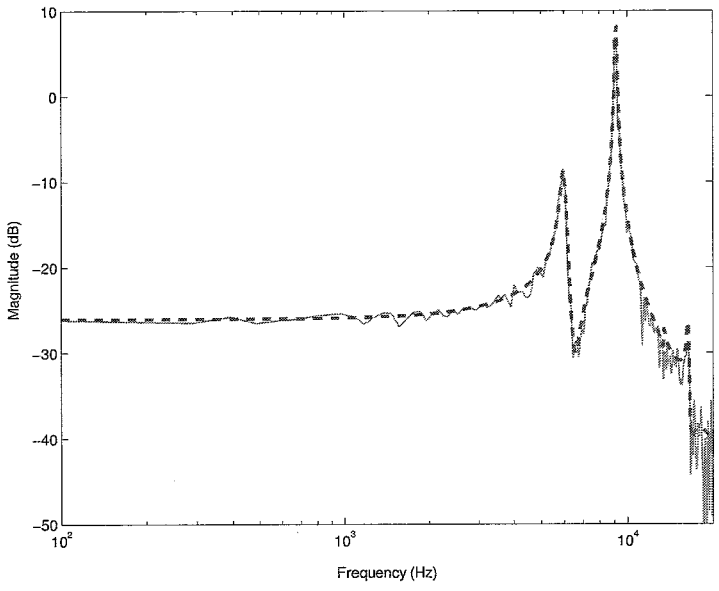

Figure B.1: Estimated (dashed) and measured (solid) frequency response of P_{ma}

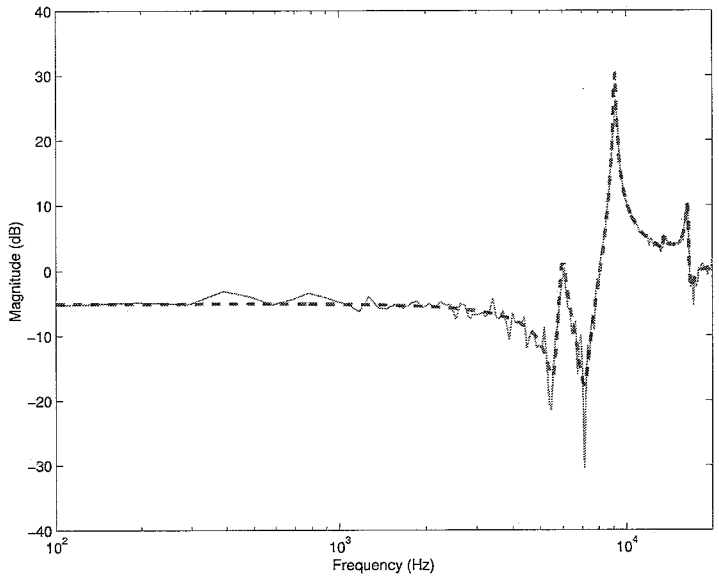

Figure B.2: Estimated (dashed) and measured (solid) frequency response of P_i

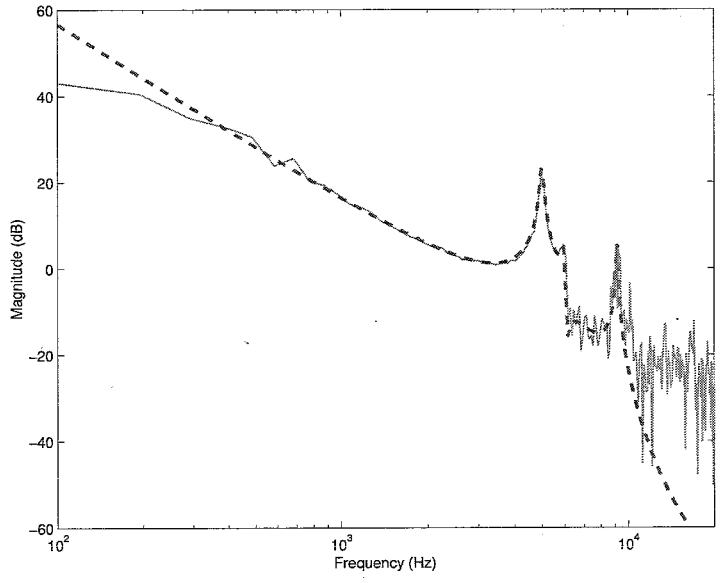

Figure B.3: Estimated (dashed) and measured (solid) frequency response of P_{vcm}

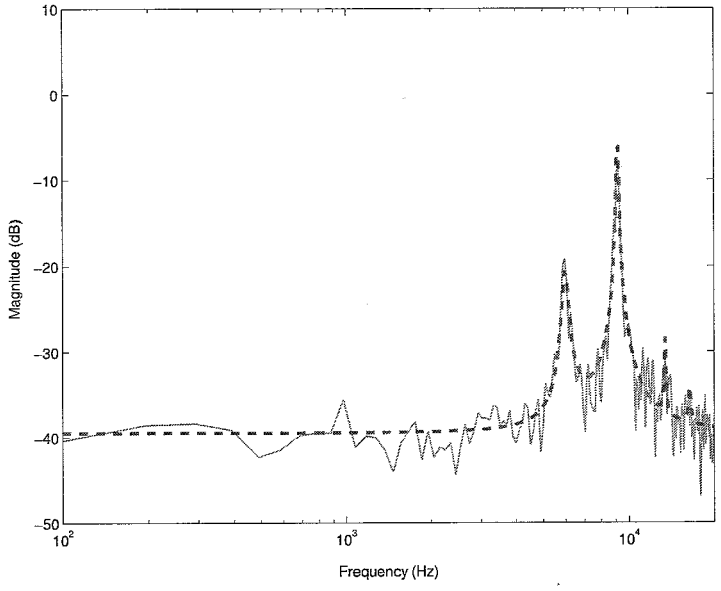

Figure B.4: Estimated (dashed) and measured (solid) frequency response of H_{ma}

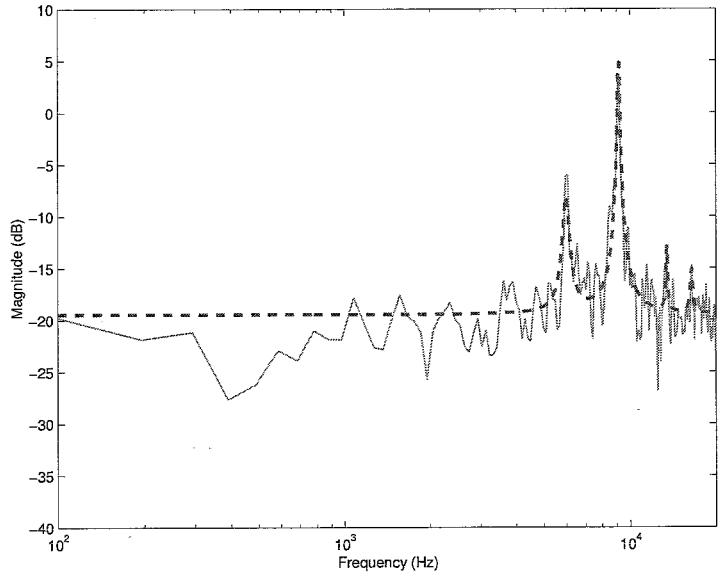

Figure B.5: Estimated (dashed) and measured (solid) frequency response of H_i

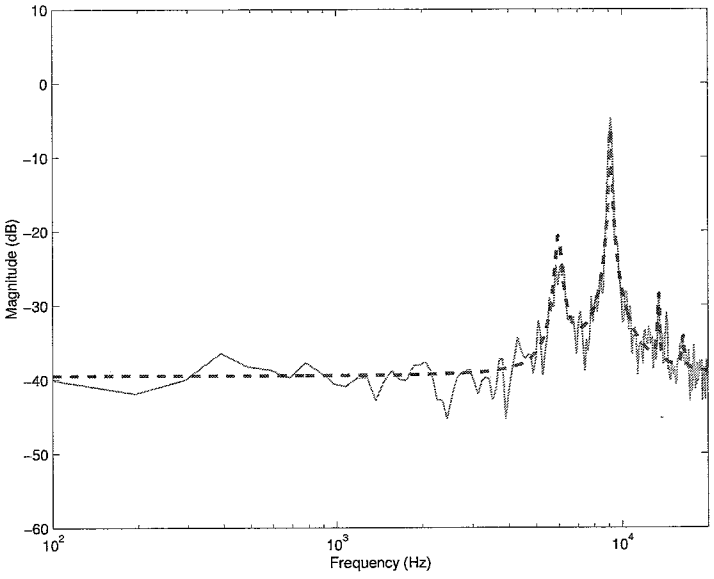

Figure B.6: Estimated frequency response of H_{ma} (dashed) and measured frequency response of H_{vcm} (solid)

Appendix C

High Bandwidth Control Loop

C.1 Closed Loop Equation

Observing figure 4.2. The equation for the input of the MA u_{ma}, including the high bandwidth control loop, is given by

$$\begin{aligned} u_{ma}(t) &= r(t) - C_i(s)H_i(s)e(t) - C_i(s)P_i(s)u_{ma}(t) \\ &= \frac{1}{1+C_i(s)P_i(s)}r(t) - \frac{C_i(s)H_i(s)}{1+C_i(s)P_i(s)}e(t) \end{aligned}$$

Here e represents the non-repeatable nature of the windage induced disturbance and r represents the control input for the MA coming from the dual stage controller C_{ds}. The PES output y_1 is given by

$$y_1(t) = H_{ma}(s)e(t) + P_{ma}(s)u_{ma}(t)$$

With the definition of u_{ma} the PES output y_1 can be given by

$$y_1(t) = F(s)r(t) + E(s)e(t)$$

where

$$\begin{aligned} E(s) &= H_{ma}(s) - \frac{P_{ma}(s)C_i(s)H_i(s)}{1+C_i(s)P_i(s)} \\ &= \frac{H_{ma}(s) + C_i(s)P_i(s)H_{ma}(s) - C_i(s)P_{ma}(s)H_i(s)}{1+C_i(s)P_i(s)} \\ F(s) &= \frac{P_{ma}(s)}{1+C_i(s)P_i(s)} \end{aligned}$$

The sensitivity function of the high bandwidth closed loop system is given by

$$S_i(s) = \frac{1}{1+C_i(s)P_i(s)}$$

The Bode diagram of controller C_i is given in section C.2 and the Bode diagram of the sensitivity function S_i is given in section C.3.

C.2 Controller C_i

C.2.1 State Space Model

$$A = \begin{bmatrix} -0.5498 & 5.747 \cdot 10^4 & 2457 & -3146 \\ -5.753 \cdot 10^4 & -15.67 & 402.9 & -217.8 \\ -7.762 \cdot 10^4 & -8439 & -8776 & -6.066 \cdot 10^4 \\ 1.377 \cdot 10^5 & 1.496 \cdot 10^4 & 6.278 \cdot 10^4 & -1.044 \cdot 10^4 \end{bmatrix}$$

$$B = \begin{bmatrix} -0.001691 \\ -0.4435 \\ -238.5 \\ 423.2 \end{bmatrix}$$

$$C = \begin{bmatrix} 1.157 & -6.172 & 26.14 & 24 \end{bmatrix}$$

$$D = \begin{bmatrix} 0 \end{bmatrix}$$

C.2.2 Bode Diagram

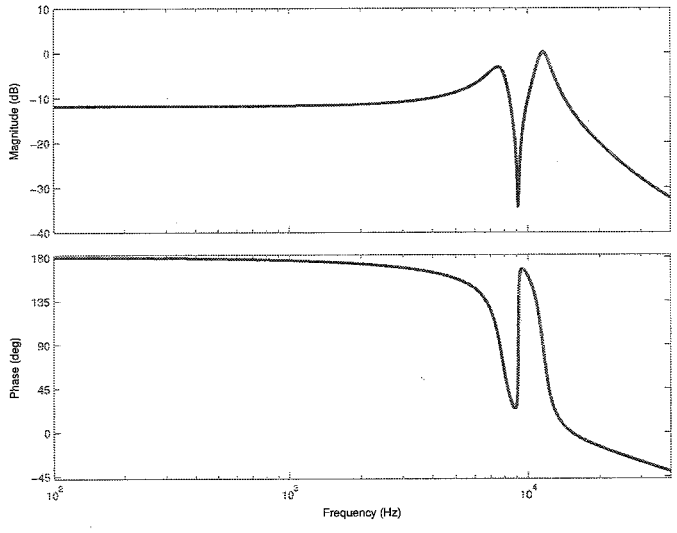

Figure C.1: Bode diagram of C_i

C.3 Closed Loop Results

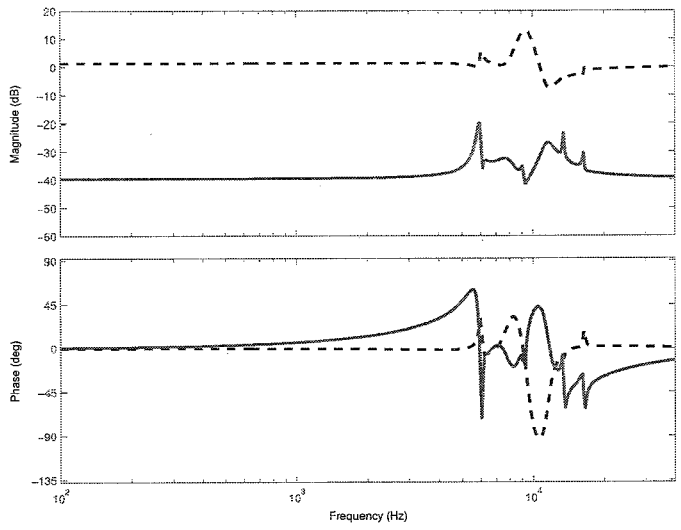

Figure C.2: Bode diagram of S_i (dashed) and $H_{ma} + C_i P_i H_{ma} - C_i P_{ma} H_i$ (solid)

C.4 Improvement Disturbance Reduction

$$
\begin{aligned}
S(s) =& \frac{1}{1 + C_0(s)C_{vcm}(s)P_{vcm}(s) + C_0(s)C_{ma}(s)F(s)} \\
=& \frac{1 + C_0(s)C_{vcm}(s)P_{vcm}(s)}{1 + C_0(s)C_{vcm}(s)P_{vcm}(s)} \cdot \frac{1}{1 + C_0(s)C_{vcm}(s)P_{vcm}(s) + C_0(s)C_{ma}(s)F(s)} \\
=& \frac{1 + C_0(s)C_{vcm}(s)P_{vcm}(s) + C_0(s)C_{ma}(s)F(s)}{\Big(1 + C_0(s)C_{vcm}(s)P_{vcm}(s)\Big)\Big(1 + C_0(s)C_{vcm}(s)P_{vcm}(s) + C_0(s)C_{ma}(s)F(s)\Big)} - \\
& \frac{C_0(s)C_{ma}(s)F(s)}{\Big(1 + C_0(s)C_{vcm}(s)P_{vcm}(s)\Big)\Big(1 + C_0(s)C_{vcm}(s)P_{vcm}(s) + C_0(s)C_{ma}(s)F(s)\Big)} \\
=& \frac{1}{1 + C_0(s)C_{vcm}(s)P_{vcm}(s)} \left(1 - \frac{C_0(s)C_{ma}(s)F(s)}{1 + C_0(s)C_{vcm}(s)P_{vcm}(s) + C_0(s)C_{ma}(s)F(s)}\right)
\end{aligned}
$$

Appendix D

Generalized System Models

D.1 Disturbance Model E

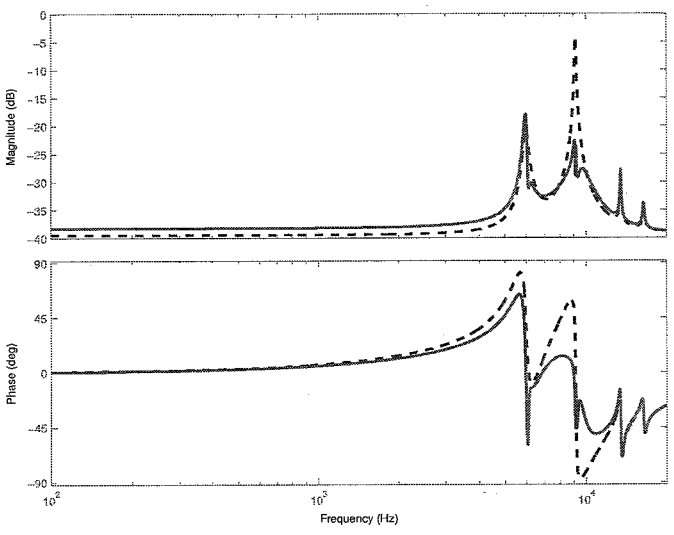

Figure D.1: Disturbance model E in configuration A (dashed) and in configuration B (solid)

D.2 System Model F

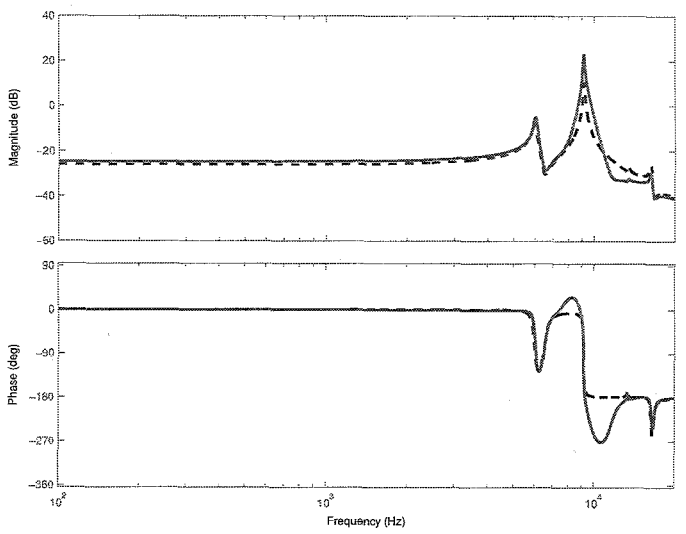

Figure D.2: System model F in configuration A (dashed) and in configuration B (solid)

Appendix E

Control Inputs

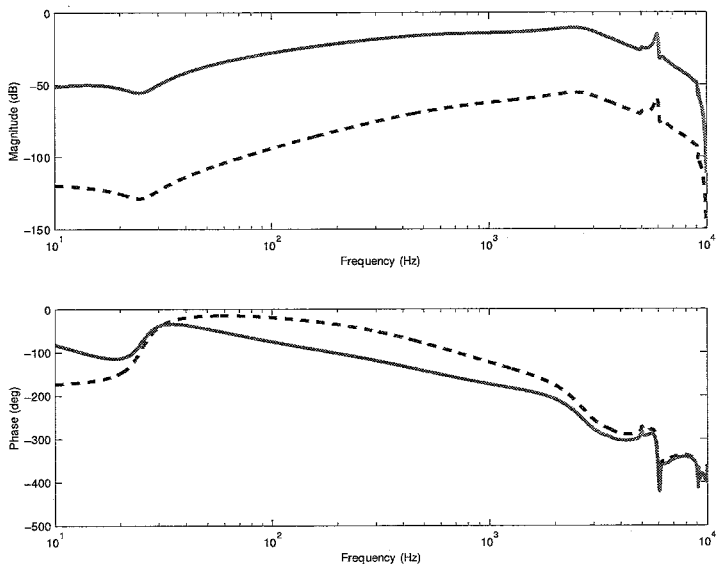

Figure E.1: Bode diagram of inputs u_{vcm} (dashed) and u_{ma} (solid)

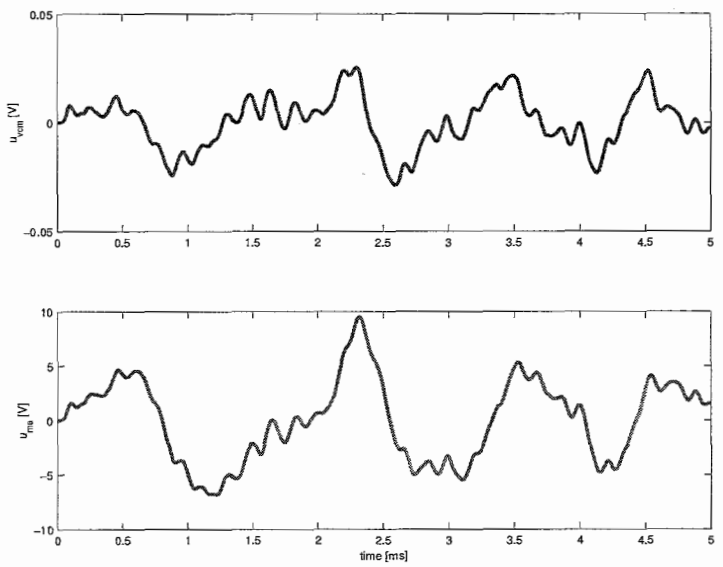

Figure E.2: Time response of inputs u_{vcm} (upper) and u_{ma} (lower)

Bibliography

[1] M. Rotunno, R. A. de Callafon, and F. E. Talke, "Comparison and design of servo controllers for dual-stage actuators in hard disk drives," *IEEE Transactions On Magnetics*, Vol. 39, No. 5, September 2003.

[2] A. P. Teerhuis, S. J. Cools, and R. A. de Callafon, "Reduction of flow induced suspension vibrations in a hard disk drive by dual stage suspension control," *IEEE Transactions On Magnetics*, vol. 8, 2003.

[3] Y. Li, and R. Horowitz, "Active suspension vibration control with dual stage actuators in hard disk drives," *Proceedings of the American Control Conference*, Arlington, VA, 2001, pp 2768-2791.

[4] N. Nilsen, and R. A. de Callafon, "Control of flow induced disturbances in a hard disk drive with a Piezo- electric Instrumented Suspension".

[5] S. J. Schroeck, W. C. Messner, and R. J. McNab, "On compensator design for linear time invariant Dual-Input Single-Output systems," *IEEE/ASME Transactions On Mechatronics*, Vol. 6, No. 1, pp. 50-57, March 2001.

[6] L. Ljung, *System Identification: Theory for the user*, Prentice Hall, Englewood Cliffs, New Jersey, 1987, ISBN 0-13-881640-9.

[7] M. Crowder, and R. A. de Callafon, "Estimation and prediction of windage induced suspension vibrations in a hard disk drive", *Journal of Information and Storage Processing Systems*, 2003.

[8] G. F. Franklin and J. D. Powell, *Digital Control of Dynamic Systems*, Addison-Wesley Publishing Company, 1980. ISBN 0-201-02891-3.